In situ measurements of Merensky pillar behaviour at Impala Platinum

by B.P. Watson*‡, J. Kuijpers*, and P. Miovsky†

Synopsis

The Bushveld platinum group metal deposits in South Africa are the largest in the world. These deposits occur as two distinct stratiform tabular ore bodies and strike for many hundreds of kilometres. Mining is extensive, with depths ranging from close-to-surface to 2300 m. The mining method is a variation of planar open stoping. Crush pillars are widely used to support the open stopes. These pillars are designed to fail and the residual strength provides the required support resistance to stabilize the stoping excavations. This paper describes the *in situ* measurement, of stress within a Merensky pillar from Impala Platinum. These measurements were used to derive a stress-strain curve that includes pre and post failure behaviour. 2D FLAC modelling, with strain softening, was done to investigate how damage expands into the hanging- and/or footwall. Although the so-called 'squat' effect is always present, the modelling suggests that it does not dominate the pillar system behaviour at larger width to height ratios. Punching of the pillar into the hanging- and/or footwall increasingly controls the pillar system behaviour with larger width to height ratios. The paper investigates the behaviour of a system that incorporates the immediate hanging- and footwall, as well as the pillar itself.

Introduction

This paper was published in the proceedings of the 42nd U.S. Rock Mechanics symposium and 2nd U.S. Canada Rock mechanics Symposium, held in San Francisco. Reprinted with permission of the American Rock Mechanics Association.

The Bushveld Complex is a large, layered, igneous intrusion which spans about 350 km from east to west. This region is situated north of the city of Pretoria in the northern part of South Africa (see Figure 1). This remarkable geological formation hosts not only the majority of the world's platinum group metals but also contains nickel and gold. There are also vast quantities of chromium and vanadium in seams parallel to the platinum ore bodies some hundreds of metres in the footwall and hangingwall, respectively. The platinum group metals are concentrated in two dipping planar ore bodies known as the Merensky Reef, a mineralized pegmatoidal pyroxenite 0.7 m to 1.4 m thick, and, underlying this, the UG2 Reef comprising one or more chromitite seams of similar thickness. The strata, generally, dip toward the centre of the complex at 8° to 15°. The *k* ratio varies from about 0.8 to over 2.5 and, locally the relatively high horizontal stress can cause severe strata control problems, particularly in tunnels. The depth of mining ranges from outcrop to 2 300 m. If a sufficiently large mining span is achieved, or the stope abuts a geological feature, a large volume of hangingwall rock can become unstable, resulting in a stope collapse, or colloquially, a 'backbreak.'

In order to prevent these backbreaks a high support resistance support system is required. This is universally achieved by the use of small in-stope chain pillars oriented either on strike for breast mining (see Figure 2) or on dip for up or down dip mining.

The pillars are known as crush pillars and they are required to fail in a stable manner soon after being cut. The residual strength of the pillars provides the required support resistance to prevent backbreaks and keep the stope hangingwall stable. These pillars provide an ideal opportunity to study the *in situ* behaviour of small pillars.

Instrument

Site description

An instrumentation site was established in a mine on the Merensky Reef in the south-west of the Bushveld Complex at a depth of 1 100 m below surface. A breast mining configuration was employed with lines of chain pillars

* *CSIR Mining Technology, South Africa.*

‡ *University of the Witwatersrand, South Africa.*

† *Impala Platinum, South Africa.*

 SA ISSN 0038–223X/3.00 + 0.00. Paper received May 2007; revised paper received May 2008.

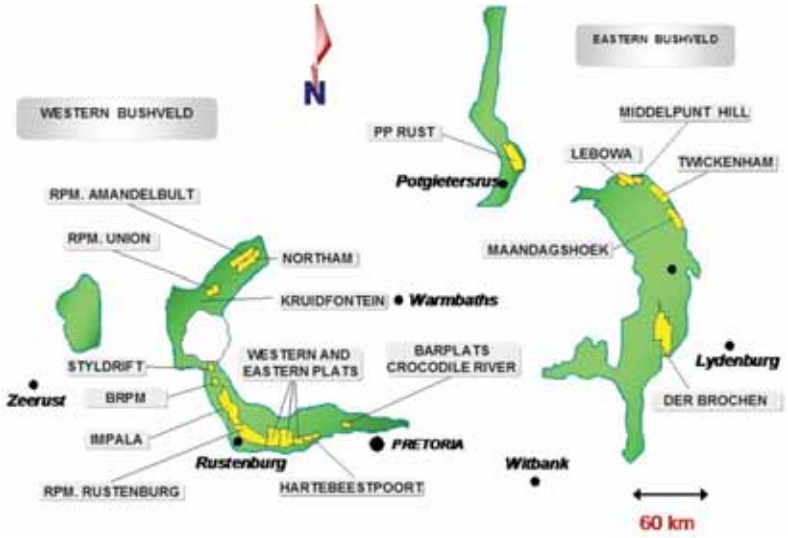

Figure 1—The extent of the Bushveld platinum exposure

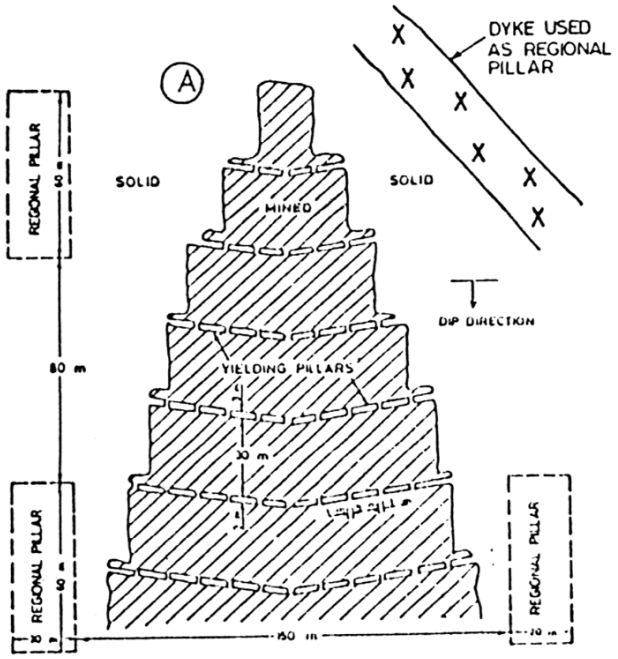

Figure 2—Plan view of a typical stope on one of the planar platinum ore bodies[1]

spaced approximately 30 m apart skin to skin (see Figure 3). The lower panel was mined in advance, specifically to allow instrumentation installation ahead of the up dip face.

Nominal pillar dimensions at the mine are 6 m x 3 m (length x width) and the stoping width is about 1.2 m. Generally, a 2 m wide siding is cut between the advanced strike gully (ASG) situated on the up dip side of the pillar and the pillar itself. This typical pillar geometry is asymmetric. Unfortunately, no siding was cut on the instrumented pillar, thus creating an abnormally large, 5 m wide pillar. The pillar length was also 5 m (slightly shorter than usual) and the height varied from 1.2 m on the down dip side to 1.8 m on the up dip side as shown in Figure 4. Although there was no siding adjacent to the monitored pillar, it can be argued that the absence of a siding has little qualitative effect on the pillar behaviour. The width: height ratio was estimated to be 3.2 using Equation [1]. The equation is based on numerical modelling performed by Roberts *et al.*[2], to account for asymmetric pillars.

$$h_c \approx \left[1 + 0.2692\left(w/h\right)^{0.08}\right]h \qquad [1]$$

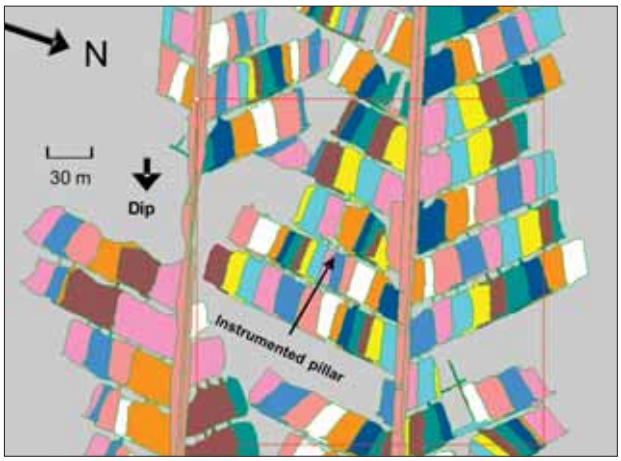

Figure 3—Mine plan showing the instrumentation site

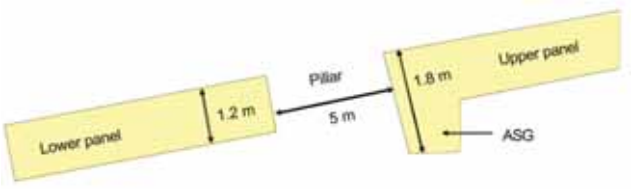

Figure 4—Section through the instrumented pillar showing the different heights on the up dip and down dip sides (not drawn to scale)

Rock behaviour

Uniaxial tests were conducted on core retrieved from the stress measurement boreholes. The scatter in results was relatively small (Figure 5) and the relationship between stress and strain was nonlinear, particularly in the direction of the applied stress. This behaviour complicated the interpretation of the stress measurements and some assumptions had to be made.

Thin sections of these nonlinear rocks and similar rocks that showed a linear elastic response were viewed under a microscope to investigate the nonlinear behaviour. No differences in mineralology or fracture density could be detected in the investigation. However, under high magnification, in a scanning electron microscope, open fractures were detected in the non linear material, but not in the linear elastic rocks. The behaviour of the non linear material and the open micro fractures appears to be explained by the concepts of 'anelastic strain recovery' (ASR)[3–5]. A hydrostatic test (Figure 6) showed that the material was softer in the axial than in the radial direction. It was assumed that the anisotropy was due to damage induced by the drill bit. The consistency in the lateral strains in the uniaxial tests, shown in Figure 5, indicates that there is uniform radial deformation around the core axis. It was, therefore, assumed that the lateral strain shown in Figure 6 is also uniform around the circumference of the core.

The results of the hydrostatic test imply that elastic constants could not be determined from the uniaxial tests; this is because the *in situ* stress measurements were conducted perpendicular to the direction of loading in the uniaxial test. The large dilation shown in the uniaxial tests indicates the opening of axial micro-fractures. This fracture opening is suppressed in the hydrostatic test. As the conditions at the measurement site are best represented by biaxial loading, it is not realistic to use the information from the hydrostatic test directly. In addition, the hydrostatic test could only be conducted at low pressures. A biaxial test (Figure 7) was, therefore, used to replicate the actual measurements, which were conducted at the flat end of a borehole. Unfortunately, these tests could also only be conducted at low pressures.

In this paper, it is assumed that the rock mass properties are uniformly distributed so that it is possible to use the laboratory results to directly evaluate the *in situ* stresses. However, if localized damage forms around the flattened end of the borehole before the strain gauges are applied, then the above assumption is invalid. Stress concentrations at the location of the strain gauges would be affected and the correlation between measured strain and *in situ* stress would be different. It is important that this possibility is considered. The nonlinear behaviour implies that the modulus changes with the level of stress. Therefore, each stress measurement is associated with a unique modulus. The modulus was based on the biaxial strains measured by the underground stress instrumentation. Therefore, the strain-stress relationship in (Figure 7) had to be extrapolated to account for the higher strains measured underground. This was done by using a hyperbolic fit originally employed by Goodman *et al.*[6] to describe a closing discontinuity under compression (also used to describe the behaviour of backfill). Equation [2] is a modified version of the original equation and accounts for the total strain (ε_t), which is the sum of the linear and nonlinear elastic response of the matrix. The 'a' value corresponds to the stress at which half the void aperture is closed and the 'b' value represents the volume of open micro fractures (voids).

$$\varepsilon_t = \frac{\sigma}{E} + \frac{b\sigma}{a+\sigma} \qquad [2]$$

The matrix modulus and Poisson's Ratio were determined

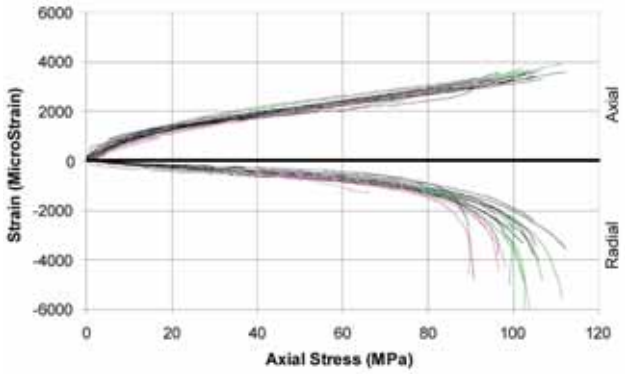

Figure 5—Strain stress curves for the uniaxial tests performed for the stress measurement evaluation (note: stress is plotted on the x-axis)

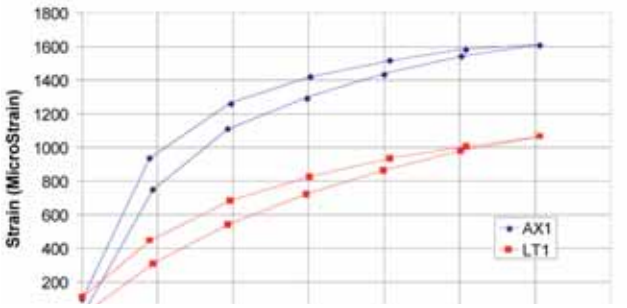

Figure 6—Strain stress curves for a hydrostatic test performed on rock core from the instrumentation site (note: stress is plotted on the x-axis)

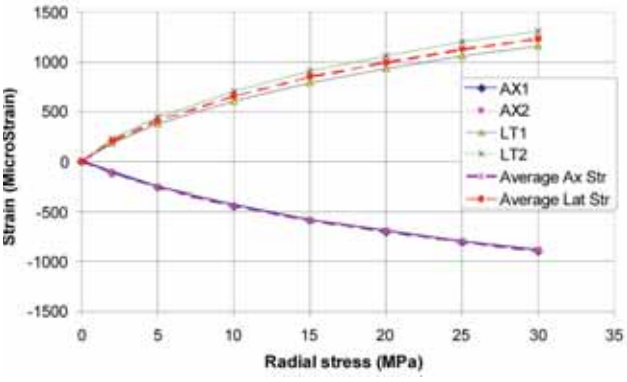

Figure 7—Strain stress curves for a biaxial test performed on rock core from the instrumentation site (note: stress is plotted on the x-axis). AX = axial direction, LT = radial direction

from high confinement triaxial tests, at axial stresses where a linear response between stress and strain was measured. The 'a' and 'b' values were determined by fitting the equation to the uniaxial test curves. The equation fitted the test data well in every case. A slight modification to Equation [2] was made to account for the Poisson effect in the biaxial test (Equation [3]). This allowed the 'a' and 'b' values to be applied to the biaxial test data and the extrapolation of the curves to higher strains (Figure 8). The biaxial curve fitting enabled a realistic representation of the biaxial stresses that were measured underground (FitLat in Figure 8).

$$\varepsilon_t = \frac{(1-\upsilon)\sigma}{E} + \frac{b\sigma}{a+\sigma} \qquad [3]$$

Instrumentation configuration

A two dimensional stress measuring cell (doorstopper) was installed above the pillar shown in Figure 9 when the mining configuration was approximately at the position indicated by '5' in the figure. A shallow-dipping borehole was drilled up from Panel 7s and the cell installed 0.74 m on the down-dip side of the proposed pillar edge as shown in Figure 10. Boussinesq[7] evaluations show that the ideal height for determining average pillar stress (APS) from a point measurement is 6 m above the pillar centre. However, the cell also measures the effects of adjacent pillars and the up-dip face from this height, which are difficult to separate in the final analysis. The installed position was a compromise to minimize errors associated with stress profile changes during the pillar evolution and adjacent face and pillar affects.

After pillar failure and once the stress had dropped to the residual strength of the pillar, a series of stress measurements were made to determine the stress profile across the pillar. These measurements were made in a shallow dipping borehole drilled about 2 m above the pillar (Figure 11), which was just above the damage zone.

Convergence was measured adjacent to the down-dip edge of the pillar but the results included heave deformations associated with foundation damage. Other instrumentation was also installed in the stope, which confirmed the date of pillar failure. Vertical boreholes were drilled in the hangingwall and footwall about 5 m down-dip of the pillar to view the foundation damage after pillar failure had taken place.

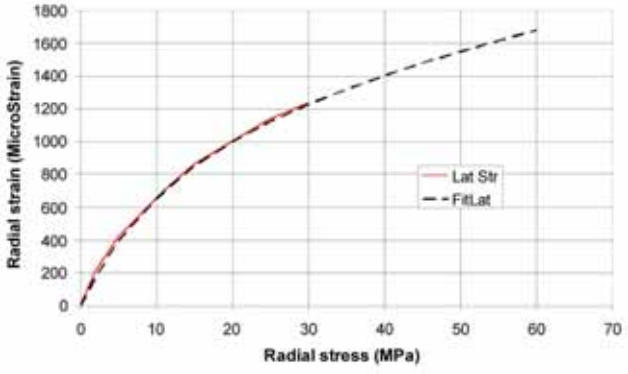

Figure 8—Extrapolated strain stress curve (FitLat) for the biaxial test shown in Figure 7 (note: stress is plotted on the x-axis)

Results

The stress cell monitoring stress change was installed ahead of the up dip face. Therefore, strain changes were measured as the stress built up in the abutment and pillar failure occurred about 2.7 m behind the face. The strains were converted to stress assuming that the rock mass was linear elastic in the region where the gauges were applied. Non linear behaviour only occurred when the stress at this point dropped to about 6 MPa. The average pillar stress (APS) was estimated using a MinSim[8] model of the mining configuration at the time of pillar failure. The ratio between the modelled APS and the modelled benchmark stress was used as a factor to quantify the *in situ* pillar stress from the measured stress. The instrumentation results and the inferred APS are shown in Figure 12.

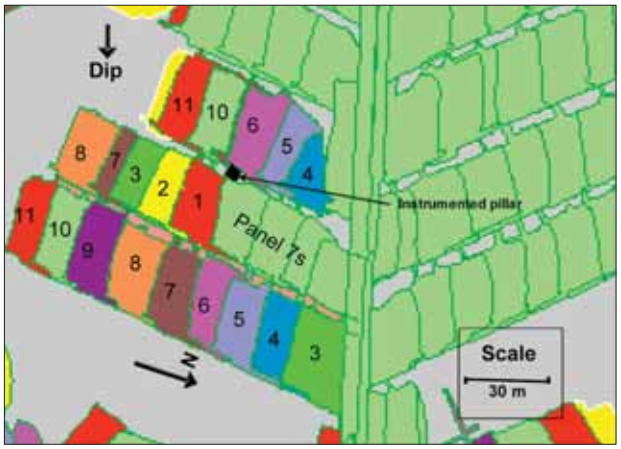

Figure 9—Stope sheet showing the mining sequence at the instrumentation site (1100 m below surface)

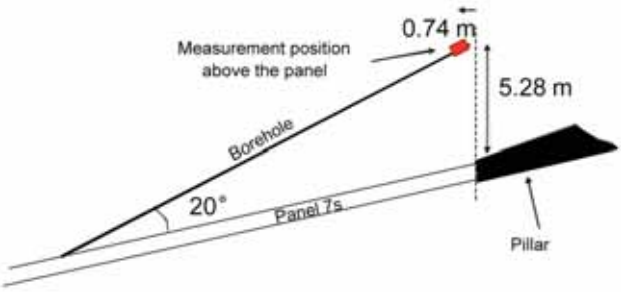

Figure 10—Section showing the stress cell position above the pillar (not drawn to scale)

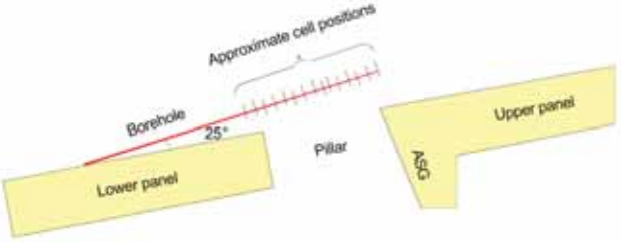

Figure 11—Section showing the asymmetric shape of the pillar and the approximate stress cell positions (not to scale)

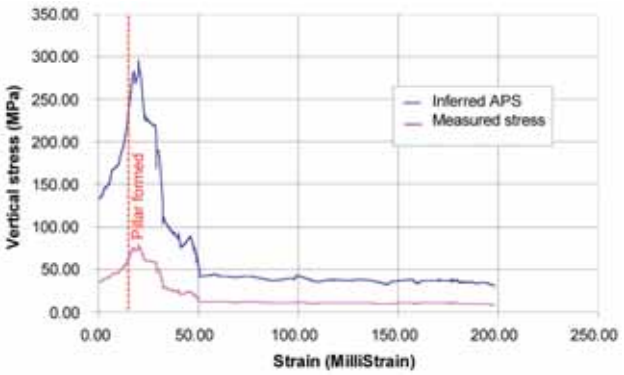

Figure 12—Stress strain curve for a 5 m x 5 m pillar (w/h ~3.2[1])

The absolute stress condition was determined from an additional strain relief measurement performed after the pillar had reached its residual strength state. This Doorstopper measurement was performed at the same height as the stress change cell. The starting stress at the measurement position was, therefore, determined by back fitting.

MinSim modelling estimated the peak strength to be about 317 MPa. This is in good agreement with the results shown in Figure 12.

The results of the stress profile measurements to determine the pillar residual strength are shown in Table I. Measurements were conducted over the 5 m wide pillar and over the stope on either side of the pillar. The stress distribution across the pillar itself was calculated using a smoothed, inverse matrix of Boussinesq[6] Equations [4], based on the measurements in the shallow dipping borehole. The equation assumes that the host rock is linear elastic.

$$\sigma_{zz} = \sum_{i=1}^{n}\left[\frac{3A_i}{2\pi} \times \frac{z_i^3}{\left(x_i^2 + y_i^2 + z_i^2\right)^{5/2}} p_{zi}\right] \quad [4]$$

Where:

σ_{zz} = stress at a point in space;

A_i = Area of the grid '*i*';

p_{zi} = Vertical stress carried by the grid '*i*'.

For the purposes of the calculations, the reef and measurements were rotated by 10° so that the top surface of the pillar could be considered horizontal. A plan view of the Boussinesq coordinate system used across the top boundary of the pillar is shown in Figure 13. The grid enabled multiple stresses to be considered across the pillar.

The reference point used for the evaluation of the stress measurements was the centre of the down dip edge of the pillar (the bottom edge in Figure 13). The matrix inversion of the measured stresses provided an unrealistic profile of pillar stresses. It was, therefore, necessary to smooth the measured profile and the estimated stress distribution across the pillar was estimated from the smoothed profile. The measurements, smoothed profile and the evaluated pillar stress profile are shown in Figure 14. The evaluation suggests a peak stress of 78 MPa at the centre of the pillar and a residual strength of about 27 MPa. Measurements were conducted at about 4 m above the pillar to confirm the residual strength estimate.

These measurements suggested a slightly higher APS of 33 MPa, which was closer to the residual strength shown in Figure 12.

Borehole camera surveys were conducted in vertical hanging- and footwall boreholes, about 5 m down-dip of the pillar, to observe the extent of the foundation damage. No fracturing was observed in the 12.5 m long borehole drilled into the hangingwall. However, significant fracturing was observed within the first 3 m of the footwall. Unfortunately water ingress through open discontinuities rapidly filled the hole with water and observations could not be made below 8 m. A further 5 shallow-dipping boreholes were drilled in the hangingwall across the width of the stope, and no fracturing was observed in any of the cores. Vertical fractures were, however, observed to a height of about 1.2 m in boreholes drilled above the pillars.

Table I

Stress profile measurements

Distance from pillar edge (m)	Height above pillar (m)	Error in strain measure (%)	Vertical stress (MPa)
-0.31	1.93	3.4	11.5
0.06	2.03	1	13.1
0.48	2.15	1.2	17.7
0.82	2.24	3.8	19.5
1.20	2.35	12.9	21.8
1.98	2.56	1.5	30.0
2.33	2.66	2.8	21.8
2.58	2.73	6.9	20.0
2.91	2.82	4.8	17.8
3.28	2.92	2.6	18.3
3.64	3.02	1.8	15.5
4.09	3.15	9.5	14.5
4.49	3.26	4.1	12.1
4.79	3.34	37.9	9.4
5.17	3.44	38.1	8.6

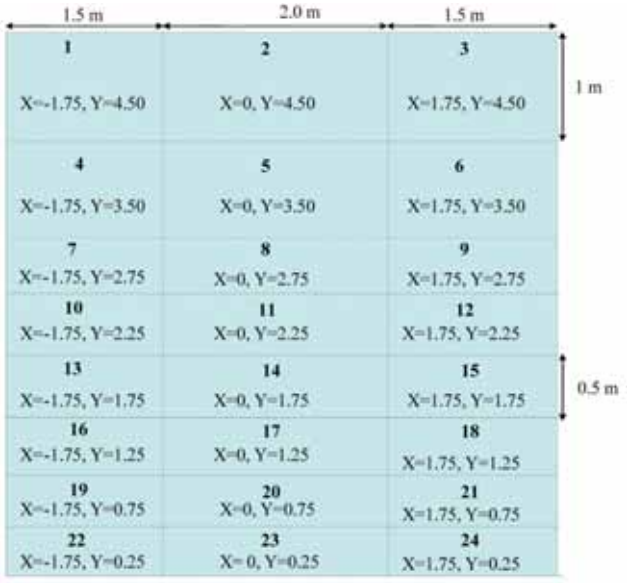

Figure 13—Plan view of the grid layout across the pillar for the Boussinesq evaluation. The origin is the centre of the bottom (down-dip edge)

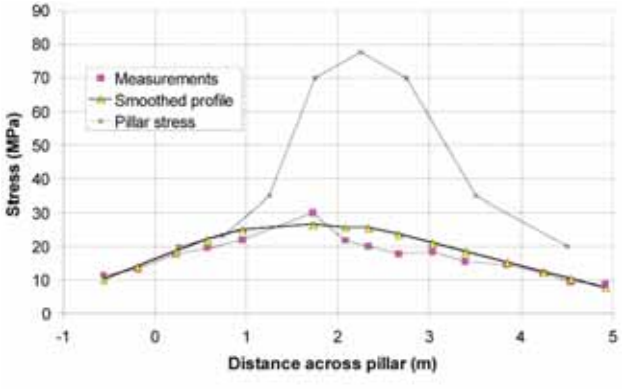

Figure 14—Comparison between the measured, smoothed and back calculated stress profiles across the pillar

FLAC Strain softening analysis

Model description

FLAC[9] was used to determine the response of a rib pillar system comprising the pillar itself and the immediate hanging and footwalls. The results of laboratory tests, in combination with previous modelling work[10] were, initially used to select parameters that control the strength and the post failure behaviour of the Merensky Reef pillars. Final parameters for the Mohr Coulomb strength criterion were calibrated from the backfit strength results of the underground pillar at the instrumentation site. As the triaxial laboratory test data showed a rapid buildup of the internal friction angle to a constant value, it was decided to represent the changes in material strength by a constant internal friction angle, combined with a linearly decreasing cohesive resistance. This allowed for a fairly simple constitutive model in which the maximum strength in the triaxial tests is determined by two constants: the internal friction angle and the initial cohesive strength. Post failure behaviour is controlled by the loss of cohesion with increasing deformation.

Boundary conditions play an important role in the punching mechanism, as they affect horizontal confinement. In the models, the vertical boundaries are not allowed to move in a horizontal direction (thereby simulating a fully replicated set of pillars). The presence of discontinuities such as bedding planes, faults and joints should also affect the punch resistance, but this was not investigated in the present study. While the numerical models provide insight into the failure mechanisms and allow quantification of the pillar system strength, it must be emphasized that these models always need to be calibrated against realistic data. Mesh density and rate of softening are important parameters in this respect and they cannot be arbitrarily selected. Table II shows the parameters that were used in the numerical model, as well as the parameters that are obtained from triaxial compression tests on pyroxenite and anorthosite. The softening rate that was used for the numerical models appears to be relatively large. Unfortunately, it was not possible to obtain realistic post failure parameters from the laboratory tests, as failure localization obscured the data.

A = anorthosite lab test
P = pyroxenite lab test
B = brittle model
S = ductile model
Co = cohesion
ϕ_0 = internal friction angle at peak load
ϕ_{res} = residual internal friction angle
ε_{pr} = residual plastic shear strain
ψ_0 = Dilation angle at peak load and
ψ_{res} = residual dilation angle.

Model results

The selected strength parameters for the Mohr Coulomb strain softening model are a cohesive resistance of 20 MPa and an internal friction angle of 40°. This results in a UCS of 86 MPa, which is slightly lower than the laboratory determined UCS (Figure 5). The rate of cohesion softening (brittleness) has a major influence on pillar strength. Failure progresses from the pillar edge towards the pillar core and is controlled, to a large extent, by the effective brittleness of the material. For example, slow failure progression will be associated with a relatively ductile material and a higher peak strength (all other parameters remaining the same). This can be appreciated from Figure 15, where two extremes were selected: a relatively brittle material with a cohesion loss of 20 MPa over 25 millistrain (brittle model), and a relatively ductile material with a cohesion loss of 20 MPa over 100 millistrain (ductile model). However, it was subsequently

Table II

Material and model properties

	σ_3 (MPa)	Co (MPa)	ϕ_0	ϕ_{res}	$\varepsilon_{pr}(m\varepsilon)$	ψ_0	ψ_{res}
A	2	15	55	50	< 0	-	-
	5	15	55	50	< 0	-	-
	10	15	55	40	< 0	-	-
P	2	16	52	50	0.75	-	-
	10	16	52	40	0.65	-	-
B		20	40	40	25	10	10
S		20	40	40	100	10	10

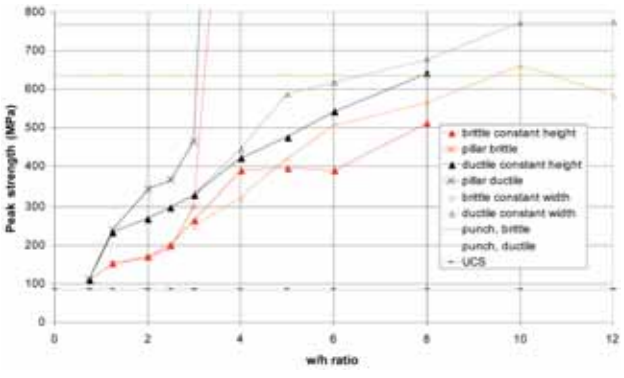

Figure 15—Effect of pillar w/h ratio for pillars that are allowed to punch, as well as for pillars that are surrounded by an infinitely strong rock mass, high density mesh and varying brittleness

found that the mesh density, or the element size, also controls the 'effective brittleness'. The results displayed in Figure 15 are obtained from models with a high mesh density in which the pillar consisted of 48 square elements across the height of the pillar, which was kept constant in the 'constant height' models.

The stope span was five times the pillar width (extraction ratio ~ 83%) and the model height was more than eight times the pillar width. The latter was varied in order to change the w/h ratio in the 'constant height' models, in which the number of elements across the width of the pillar increased proportionally. In order to investigate the possibility of this affecting punch resistance, another set of models, the 'constant width' models, was analysed. In these models, the height of the pillars was varied by using the same number of elements across the height (48), while changing the shape of the pillar elements from square to rectangular. All results are displayed in Figure 15, where it can be seen that the differences between the 'constant height' and 'constant width' width models are relatively small. This is because an increase in mesh density does not have a substantial effect on punch resistance, once a certain mesh density is exceeded. The graphs labelled 'pillar brittle' and 'pillar ductile' refer to models in which the hanging and footwall material is not allowed to fail, so that punching is not possible and failure is concentrated in the pillar. Figure 15 also shows the pillar UCS, along with the ultimate punch resistance for these relatively brittle and ductile materials. These are labelled 'punch brittle' and 'punch ductile'. As the graphs are based on a UCS of 86 MPa, a change in the value of the UCS would affect the values in the graphs proportionally.

While the softening rate (brittleness) and mesh density affect the effective pillar brittleness and consequently the effect of width-to-height ratio on strength, the mesh density also affects the punching potential of the pillar models. Models with a relatively high mesh density show a change in the mode of pillar failure once the pillar w/h ratio exceeds a certain value. At smaller w/h ratios, the pillars fail by progressively crushing from the edges towards the core, but in the wider pillars additional fracturing of the hanging- and/or footwall rock is initiated. Figure 15 shows that there is a disparity between the strengths of pillars with and without elastic foundations. This suggests that punching is initiated once the strength exceeds 250 MPa (~3 x UCS).

If the hanging- and footwall material is relatively strong and failure is restricted to the pillar, the pillars become virtually indestructible at a width-to-height ratio in excess of 3.0 (the so-called 'squat' pillar effect, normally assumed at a width-to-height ratio of 5.0). The graphs labelled 'pillar ….' in Figure 15 illustrate this effect. Laboratory experiments on hard rock pillar specimens, loaded between steel platens, have not demonstrated such an extreme exponential relationship between w/h ratio and strength. However, it should be emphasized that the boundary conditions in such laboratory experiments are not representative of in-stope pillars. The interface between the loading platen and the specimen provides limited friction[11] while the draping effect of the stope is not represented. As a consequence, the laboratory specimens experience far less confinement than the in-situ pillars and numerical modelling results are probably more representative of actual pillar behaviour.

A more realistic model includes the presence of the hanging and/or footwall. In such a model the fracturing or damage can expand beyond the pillar itself. This 'punching' phenomenon becomes an important aspect of the failure mechanism of the pillar system, and effectively controls the pillar strength at larger width to height ratios. The graphs in Figure 15 suggest an approximately linear increase in pillar strength with an increasing w/h ratio. At relatively large w/h ratios, the punch resistance does, however, reach a maximum at stress levels of 630 MPa and 780 MPa for the brittle and ductile materials respectively, as shown in the figure. These levels indicate the ultimate punching resistance of infinitely stiff and strong pillars.

The fact that material brittleness has such a profound effect on system strength can be explained on the basis of the pillar failure process. Unlike in triaxial tests, where uniform stress conditions (USC) prevail prior to specimen failure, pillar failure initiates at the pillar edges and progresses gradually towards the core of the pillar. Edge failure typically starts at a relatively low average pillar stress. Failure progression towards the pillar core is to a large extent controlled by the post failure behaviour of the previously failed material near the pillar edge. A relatively ductile material would provide more resistance during its post failure degradation, as it requires more deformation to become completely destroyed. Pillar failure progression will therefore be more restrained in the case of a more ductile material as compared to a more brittle material. This implies that an increasing pillar width to height ratio will be associated with a larger rate of strength increase in the case of a relatively ductile material, while the rate of strength increase will be minimal in the case of a very brittle material. This is consistent with the non punching pillar results shown in Figure 15.

The relationship between pillar strength and width to height ratio is likewise influenced by mesh density. At higher densities, an increase in width to height ratio brings with it less of an increase of strength. This can be explained by the fact that an increased mesh density leads to an increase in effective brittleness. Fracture localization is enhanced in the case of a denser mesh which implies that foundation fracturing is more likely to occur in a model with a fine mesh than in a model with a coarse mesh. However, foundation fracturing is not synonymous with foundation failure. Foundation failure is the final stage, in which vertical punching is accommodated by horizontal dilation. It appears that this dilation is induced at a lower resistance level when the element sizes are relatively large. In other words, a reduction in element size (and therefore, an increase in mesh density) would cause an increased punch resistance. This is in opposition to the effects of mesh density on the crushing of the pillar itself and on foundation fracturing.

In order to obtain a representative material brittleness as well as a correct correlation between pillar failure and rock mass failure, the combination of mesh density and rate of cohesion softening needs to be calibrated properly. Most appropriate, obviously, would be the combination which results in the most accurate estimates of a wide range of pillar strengths. Figures 16 to 18 show the load deformation characteristics and failure distributions for various pillar geometries, mesh densities and cohesion softening rates. The APS in Figures 16 and 17 were compared to deformations adjacent to the edge of the pillars (closure), in a similar location to the underground measurements.

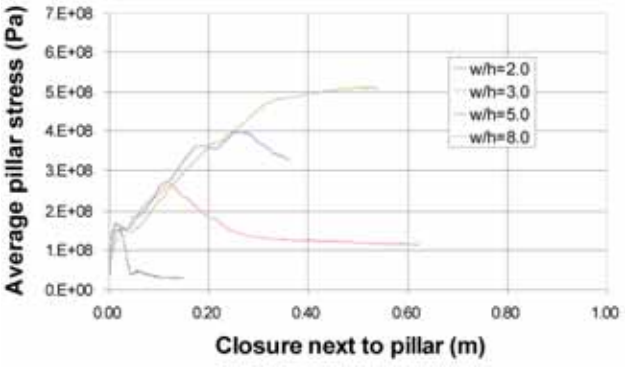

Figure 16—Load deformation relationship for various w/h pillars; dense grid and most brittle material

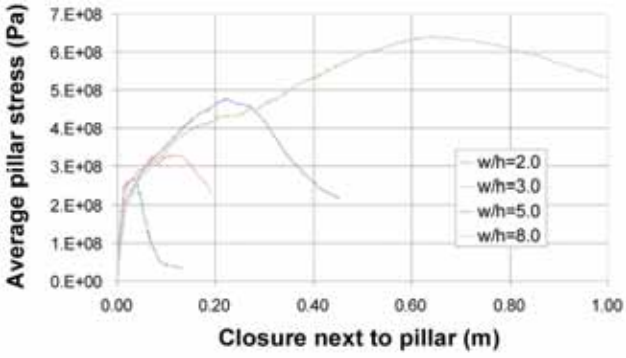

Figure 17—Load eformation relationship for various w/h pillars; dense grid and least brittle material

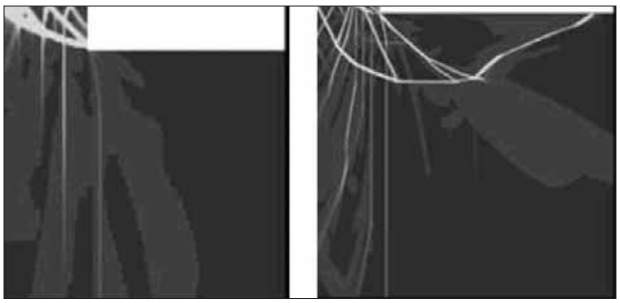

Figure 18—Failure distribution, using dense mesh and ductile material, w/h = 2.0 (left) and 5.0 (right) (double symmetry)

It is of interest to note that the pillar with a w/h ratio of 2.0 is completely crushed, with limited failure in the footwall, while the pillar with a w/h ratio of 5.0 shows extensive footwall failure combined with relatively large solid wedges in the core of the pillar. The typical 'Prandtl wedge'[12] formed in the footwall causes the footwall material to dilate into the stope, therefore, accommodating the actual pillar deformation and failure. Failure of a pillar system, which includes the adjacent footwall and/or hangingwall rock, involves, in essence, a combination of three mechanisms. First, there is fracturing and crushing of the pillar itself, which often is reproduced under laboratory conditions with unrealistic boundary conditions. Then, there is the fracturing into the surrounding material, the Herzian[13] crack and wedge formation. The third mechanism is the horizontal dilation of the foundation, which controls the ultimate resistance against punching. These latter two mechanisms have only been investigated to a very limited extent as far as brittle materials are concerned and references are therefore sparse (Cook *et al.*[14], Dede[15], Özbay and Ryder[16], Wagner and Schümann[17]). It is, however, clear that the failure of realistic pillar systems, with the probable exception of very slender pillars in hard rock, is to a large extent controlled by the fracture and failure processes in the foundation. This was also reported by Lenhardt and Hagan[18] who observed foundation failure in a pillar at Western Deep Levels Gold Mine. These processes, therefore, need to be included in any realistic analysis.

Discussion

The stress strain curve for the more brittle FLAC model (Figure 16) provided a close correlation to the measured strength (Figure 12) but the post failure strains were significantly higher in the model. The size, and resultant strength, of the instrumented pillar prevented failure from occurring at the face, which means that failure took place under relatively soft loading conditions. The soft loading conditions are believed to be partly responsible for the more rapid drop in stress and the comparatively low final residual strength of the monitored pillar. The vertical fractures shown in the model (Figure 18) were observed in the hangingwall but the shallower 'Prandtl wedge'[12] type fractures did not form over the stope. However, these fractures may have formed in the footwall.

The model suggests that small pillars with a w/h ratio of less than 2.0 are likely to create little or no foundation failure. The residual strength of these pillars will be lower than the standard pillars, but there is evidence that even pillars with a w/h of 1.5 are sufficiently strong[19] under normal mining configurations. However, more work is required to determine the w/h effects on residual strength and what the influences of loading conditions are.

The results of the numerical modelling, clearly show that pillars need to be viewed as a system that incorporates the immediate hanging and footwall, as well as the pillar itself. With increasing w/h ratio, failure is not contained solely within the pillar, but also expands into the hanging and/or footwall. The so-called 'squat' effect is still present, but it no longer dominates the pillar system behaviour. Increasing pillar strength and pillar load results in increasing damage and failure in the hanging and/or footwall. The ultimate punch resistance is reached when the w/h ratio approaches 10. Therefore, no benefit with respect to preventing pillar failure is gained by cutting pillars larger than this ratio.

Material brittleness has a profound effect on system strength. Less brittle materials create stronger pillars because they provide more resistance during post failure degradation. Pillar failure progression is more restrained in the case of a more ductile material as compared to a more brittle material. This implies that an increasing pillar width to height ratio will be associated with a larger rate of strength increase in the case of a relatively ductile material, while the rate of strength increase will be lower in the case of a very brittle material.

The residual strength of the monitored pillar was between

27 MPa and 33 MPa, which was significantly greater than the 13 MPa requirement[20]. This suggests that a smaller pillar would have been sufficient. The relatively high stress at the centre of the pillar caused a time dependant deterioration of the fractured rock immediately adjacent to the pillar, which resulted in the detachment of small bocks around the pillar as shown in Figure 19.

The stress distribution shown in Figure 20 is similar to the Wagner[21] profile for a failed coal pillar (profile 3 in Figure 21). The comparison suggests that the monitored pillar has not reached its residual strength and may reduce further with time. However, the stable stress condition shown in Figure 12 did not change over a period of 1.4 years during which time significant mining took place.

Conclusion

The residual strength of the instrumented crush pillar (w/h~3.2) was between 27 MPa and 33 MPa, which was significantly greater than the requirement. The modelling suggests that little or no foundation failure will occur if the w/h is less than 2, as the pillar will fail at relatively low stresses. Therefore, more stable conditions are likely with small pillars, particularly in poor ground conditions but more work is required to establish the relationship between w/h and residual strength for proper crush pillar design. In addition, there may be an effect of loading condition on residual strength which needs further investigation. The stress strain relationship of the monitored 5 m x 5 m pillar was determined. The peak strength of about 300 MPa, was also confirmed by MinSim modelling.

The results of the numerical modelling and the instrumentation show that pillars are part of a system that incorporates the immediate hanging and footwall, as well as the pillar itself. With increasing w/h ratio, failure is not contained solely within the pillar, but also expands into the hanging- and/or footwall. The so-called 'squat' effect is still present, but it no longer dominates the pillar system behaviour. Increasing pillar strength and pillar load results in increasing damage and failure in the hanging and/or footwall. The ultimate punch resistance is reached when the w/h ratio approaches 10. Thus no benefit is gained by cutting pillars larger than this ratio. The brittleness of the rock affects the peak strength with less brittle materials forming stronger pillars.

Acknowledgement

This paper was published in the proceedings of the 42nd US Rock Mechanics Symposium.

Figure 19—Down-dip edge of the pillar, showing the hangingwall blocks that fell out as a result of time dependant hangingwall deterioration adjacent to the pillar

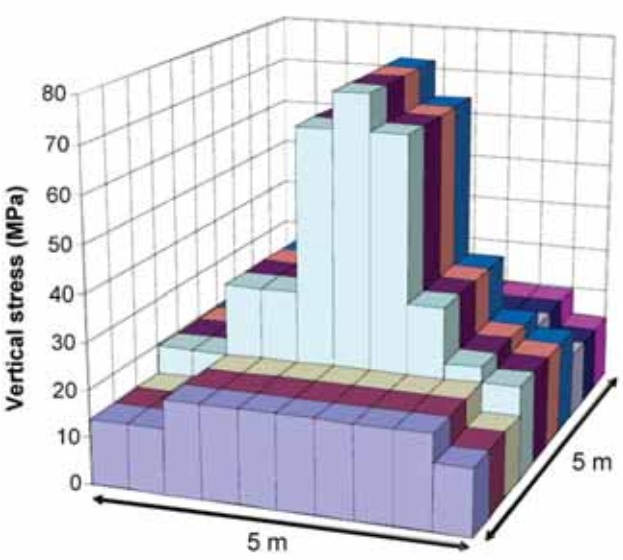

Figure 20—Stress profile across the instrumented pillar (produced by the Boussinesq inverse matrix)

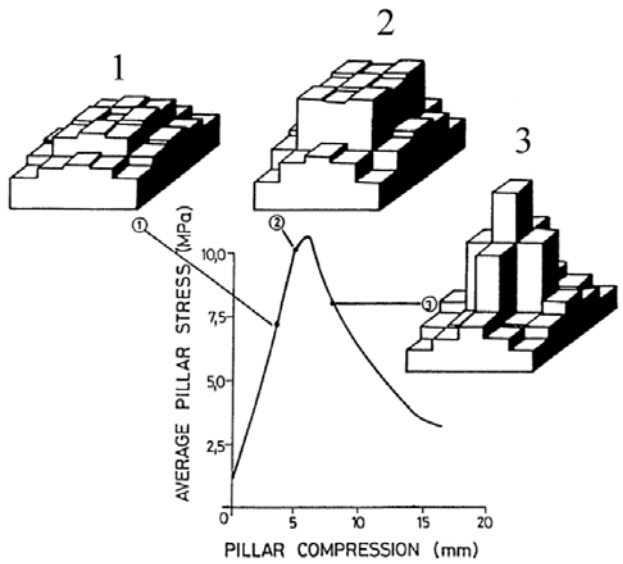

Figure 21—Wagner's[21] *in situ* tests on coal pillars, showing the stress profile across a pillar for three APS levels (1=elastic, 2=yield and 3=post failure)

References

1. Ozbay, M.U. and Roberts, M.K.C. Yield Pillars in Stope Support. *Rock Mechanics in Africa*. SANGORM Congress. 1988.
2. Roberts, D.P., Canbulat, I., and Ryder, J.A. Design parameters for mine pillars: strength of pillars adjacent to gullies; design of stable pillars with w/h ratio greater than 6; optimum depth for crush pillars. *SIMRAC GAP617 Final Report*. SIMRAC. Johannesburg. 2002.
3. Walsh, J.B. The effect of cracks on the uniaxial compression of rocks. *J. Geophys. Res.* vol. 70, no. 2, 1965. pp. 399–411.
4. Bristow, J.R. Microcracks and the static and dynamic elastic constants of annealed and heavily cold-worked metals. *Brittish J. Appl. Phys.*, vol. 11, 1960. pp. 81–85.
5. Kachanov, M. Effective elastic properties of cracked solids: critical review of some basic concepts. Appl. Mech. Rev., vol. 45, no. 8, 1992. pp. 304–335.
6. Goodman, R.E., Taylor, R.L. and Brekke, T. A model for mechanics of jointed rock. *J. of Soil Mechs & Foundation Div.*, Proc. ASCE 94, SME3. 1968.
7. Poulos, H.G. and E.H. Davis. *Elastic solutions for Soil and Rock Mechanics*. J Wiley& Sons. N. 1974.
8. COMRO. MINSIM-D User's Manual, *Chamber of Mines of South Africa*, Johannesburg. 1981.
9. Itasca consulting group, inc. *Fast Lagrangian Analysis of Continua (FLAC)*, Vers. 3.2. Minneapolis Minnesota USA. 1993.
10. Watson, B.P., Kuijpers, J. Nkwana, M.M., and Van Aswegen, L. The stress–strain behavior of in–stope pillars in the Bushveld Platinum deposits in South Africa. *J. South African Inst. Min. and Met*, vol. 107, 2007.
11. York, G. Numerical modeling of the yielding of a stabilizing pillar/foundation system and a new design consideration for stabilizing pillar foundations. *J. South African Inst. Min. and Met.* vol. 98: 1998. pp. 281–293.
12. Prandtl, L. *Zeit.Angew.Math. Mech.* vol. T, no. 1, 1921. pp. 15–20.
13. Hertz, H. On the contact of rigid solids and on hardness, miscellaneous papers, Macmilan, London. 1986.
14. Cook, N.G.W., Hood, M., and Tsai, F. Observations of crack growth in hard rock loaded by an indenter. *Int. J. Rock Mech. Min. Sci. & Geomech. Abstr.*, vol. 21, no. 2, 1984. pp. 97–107.
15. Dede, T. Fracture onset and propagation in layered media. MSc dissertation, University of the Witwatersrand, Johannesburg. 1997.
16. Özbay, M.U. and Ryder, J.A. The effect of foundation damage on the performance of stabilizing pillars. *J. South African Inst. Min. and Met.*, vol. 90, no. 2, 1990. pp. 29–35.
17. Wagner, H. and Schümann, E.H.R. The stamp-load bearing strength of rock. An experimental and theoretical investigation. *Rock Mechanics*, vol. 3, 1971. pp. 185–207.
18. Lenhardt, W.A. and Hagan, T.O. Observations and possible mechanisms of pillar associated seismicity at great depth. Proc. International Deep Mining Conference, Johannesburg, South Africa. *J. South African Inst. Min. and Met. Symposium series S10*, 1990. pp. 1183–1194.
19. Korf, C.W. Stick and pillar support on Union Section, Rustenburg Platinum Mines. *Association of Mine Managers of South Africa*. 1978. pp. 71-82.
20. Roberts, D.P., Roberts, M.K.C., Jager, A.J., and Coetzer, S. The determination of the residual strength of hard rock crush pillars with a width to height ratio of 2:1. *J. South African Inst. Min. and Met.* 2005. vol 105, pp. 401–408.
21. Wagner, H. Pillar design in coal mines. *J. South African Inst. Min. and Met.* January. 1980. pp. 37–45. ◆